Journal of Engineering Mechanics and Machinery (2023)
Clausius Scientific Press, Canada

DOI: 10.23977/jemm.2023.080105
ISSN 2371-9133 Vol. 8 Num. 1

Research on transverse impact performance of pipe-in-pipe structure

Xin Hu

Beijing University of Technology, Beijing, 100124, China

Keywords: Pipe-in-pipe structure; transverse impact; numerical simulation; dynamic response

Abstract: Pipe-in-pipe structure are widely used in offshore oil and gas transportation. The structure is subjected to various dynamic loads such as earthquakes and vortex-induced vibrations during service, of which transverse impact is the main cause of structure damage. At present, the whole process analysis and parameter analysis of the pipe-in-pipe structure under the action of impact are not systematic and complete. Based on the explicit dynamic software LS-DYNA, the finite element model of the pipe-in-pipe structure was established, and a systematic parametric analysis was carried out on the parameters of the pipe-in-pipe structure. Based on the three aspects of force, displacement and energy absorption, the influence of the three parameters of span, diameter ratio and thickness ratio on the impact resistance of the tube-in-tube structure is revealed. The research results show that the impact force time-history curve of the pipe-in-pipe structure can be divided into five stages. The resistance of the tube-in-tube structure to impact is significantly influenced by the ratio of thickness and span.

1. Introduction

Currently, the development of offshore oil and gas resources has shifted from nearshore to deep sea. As a crucial equipment for transporting marine oil and gas, the importance of subsea pipelines is increasingly emphasized. Because the pipe-in-pipe structure has good thermal insulation properties, this structure is widely used in submarine pipelines. The pipe-in-tube structure is composed of an inner pipe used for hydrocarbon transportation and an outer pipe for protection. The annular space or non-structural insulation material is filled between the inner and outer pipes. The stabilizer is usually made of polymer and is clamped onto the inner pipe at certain intervals to ensure concentricity between the inner and outer pipes. As the number of subsea oil and gas transportation pipelines increases rapidly, the probability of being laterally impacted by anchors, trawl gears and other heavy objects also increases. According to the report on subsea pipeline failures by the American Gas Association (IAGA) [1], external impact is the main cause of subsea pipeline failures, accounting for 47% of the failure rate. Therefore, it is of great significance to study the lateral impact performance of the pipe-in-pipe structure.

Numerous studies have investigated the effects of lateral impact on submarine pipelines, with a primary focus on single-wall pipe structure. Single-walled pipes refer to metal pipes with a single layer of wall responsible for transporting and resisting external impact loads. For the study of impact

behavior on underwater pipes caused by falling objects such as anchors, sunken ships, navigation debris, etc., both domestic and foreign scholars have primarily utilized theoretical, experimental, and numerical simulation approaches for single-walled pipes. Jones et al. [2] conducted lateral impact experiments on steel pipes clamped at both ends. Jones and Shen [3] further studied steel pipes clamped at both ends under lateral impact and proposed a theoretical method for rigid-plastic solutions. By enabling the sustained evolution of local pipeline deformation throughout the general deformation phase, this technique ensures that the analysis outcomes align more cohesively with the highest permanent lateral displacement observed in the experiment. Based on the cross-sectional shape in [2, 3], Chen and Shen [4] obtained the initial impact energy threshold that caused material fracture. In a study by Chen and Shen [5], an assortment of experiments were carried out on steel pipes clamped at both ends and subjected to lateral impact. The research delved into the influence of pipeline geometry, fluid pressure, and point of impact on the threshold of impact energy. Cerik et al. [6] conducted a large number of numerical simulations and classified the force-displacement curves of pipelines subjected to low-speed impacts. In a study by Zhu et al. [7], steel pipes clamped at both ends were subjected to low-speed lateral impact experiments, and a straightforward technique for determining the local dents and overall deformation of the pipes was put forward. Zhang et al. [8] conducted hammer and quasi-static tests on circular steel pipes and found that steel pipes clamped at both ends undergo deformation according to the three-hinge mechanism under lateral load. In a study by Liu et al. [9] and Lu et al. [10], experiments and numerical analyses were respectively carried out on the t-shaped and k-shaped pipe nodes of offshore platforms under lateral impact. This led to the acquisition of the force-displacement relationship for impact corresponding to the different pipe structures.

During transportation, single-walled pipes cannot prevent heat transfer between oil and gas and seawater, resulting in the formation of solid hydrates of hydrocarbons at low temperatures. Due to its excellent insulation properties, the pipe-in-pipe structure has found extensive application in transporting natural gas and oil through pipelines. The instability of the pipe-in-pipe structure has been the primary focus of prior research efforts. For example, previous studies on the propagation of buckling in the pipe-in-pipe structure [11-13] were conducted through experiments and numerical simulations, and theoretical and numerical studies were conducted on various vibrations that cause free spans in the pipe-in-pipe structure [14,15]. In terms of impact, Zheng et al. [16-19] conducted experiments and numerical simulations on the pipe-in-pipe structure, studying its ability to resist impacts and drags from trawling gear and its transverse impact resistance under external pressure. Through a series of drop hammer impact tests and finite element simulations, Gao et al. [20] conducted a comparative analysis of the response of single-walled pipes and pipe-in-pipe structures to lateral impact. The results revealed that the pipe-in-pipe structure demonstrated superior impact resistance. In their study, Gao et al. [21] examined the impact of span, corrosion, and dent defects on the transverse impact toughness of pipe-in-pipe structures that had been in service for a period of 15 years. This article simulates the experiment by Zheng et al. [12] and conducts two studies: (1) analysis of the entire process of impact force acting on the pipe-in-pipe structure; (2) study of key parameters of the steel pipe, namely span, diameter ratio, and thickness ratio.

2. Finite element model of the pipe-in-pipe structure

2.1 Information on pipe-in-pipe structure impact test

Zheng et al. [12] evaluated the transverse impact on the articulated support of the pipe-in-pipe structure through a test. The experimental setup, as shown in Figure 1(a), mainly included steel blocks and a hammerhead, a pipeline support system, and a pipe-in-pipe structure. The combined mass of the hammerhead and steel block was 1350kg, and they were capable of sliding vertically along the

guide rail. The hammerhead was wedge-shaped with a radius of 30mm. As shown in Figure 1(b), an Omega component was set at the support end to prevent the pipeline from bouncing after being impacted. A schematic illustration of the pipe-in-pipe structure was presented in Figure 1(c), which showed the installation of a 50mm aligner at each end of the inner pipe to maintain its center position. Table 1 presents the detailed specifications of the pipe-in-pipe structure. The outer pipe's outer diameter is represented as D_o, while its thickness is represented as t_o. Similarly, the inner pipe's outer diameter is represented as D_i, and its thickness is represented as t_i. The span is denoted as L, the weight of the hammer as m_d, and the drop height as h.

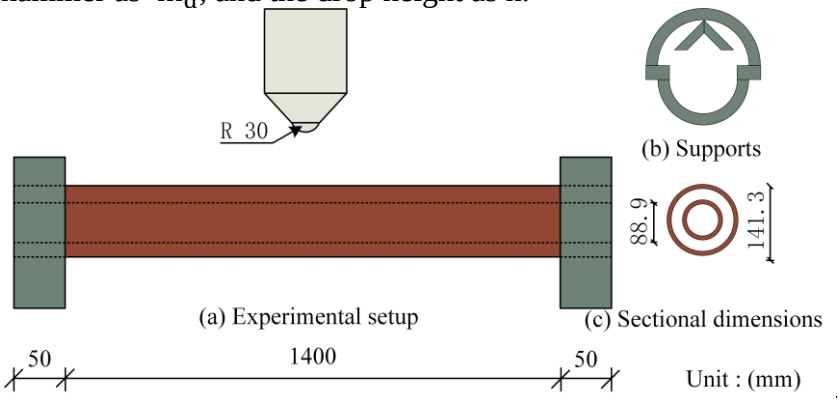

Figure 1: Experimental schematic diagram

Table 1: Experimental Setup Parameters

D_o/mm	t_o/mm	D_i/mm	t_i/mm	L/m	m_d/kg	h/m
141.3	6.55	88.9	5.49	1.5	1350	0.5

2.2 Establishment of finite element model for pipe-in-pipe structure

Using LS-DYNA software, we simulated the pipe-in-pipe structure's dynamic response to a falling hammer while supported by articulated ends on both sides. The numerical model of the pipe-in-pipe structure created using the parameters outlined in Section 1.1 is depicted in Figure 2.

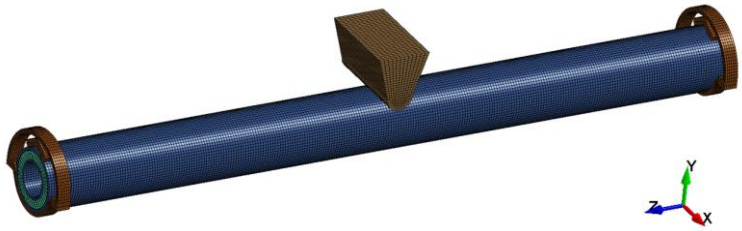

Figure 2: Finite element model

2.2.1 Element type and mesh size

The pipe-in-pipe structure's exterior and interior pipes, along with its stiffeners, supports, and falling hammer, were modeled using the SOLID_164 eight-node hexahedral solid element with single-point integration. The computation cost was reduced and accurate results were obtained by appropriately controlling the hourglass effect. The mesh convergence was studied, and a mesh size of 6mm was chosen to balance accuracy and computational efficiency. In the simulation of the falling hammer, only the hammerhead was modeled, and the density of the falling hammer was adjusted to match that used in the experiment.

2.2.2 Material model

For the exterior and interior pipes, we opted for the *MAT_024 material model, also known as *MAT_PIECEWISE_LINEAR_PLASTICITY. This model allows for input of the stress-strain curve to account for the nonlinear behavior of the steel material, while also considering strain rate effects. To account for the effects of strain rate on the steel material, we employed Cowper-Symonds model's formula (1) as outlined in [22].

$$\sigma_{dy} = \sigma_y \left(1 + \frac{\dot{\varepsilon}}{C}\right)^{\frac{1}{p}} \tag{1}$$

The equation assigns constants C and p, as well as steel's dynamic yield strength σ_{dy}, static yield strength σ_y, and strain rate $\dot{\varepsilon}$. Incorporating Abramowicz and Jones' empirical values[23] of 6844.1 and 3.91, respectively, we determined the appropriate values for the pipe-in-pipe structure design.

For improved computational efficiency, we selected the *MAT_020 (*MAT_RIGID) material model and assumed that both the falling hammer and the supports were rigid bodies. The stiffeners were made of nylon material, and the Young's modulus, which was found from the product data sheet, was 37MPa. Therefore, the material model *MAT_001 (MAT_ELASTIC) was chosen for the stiffeners.

2.2.3 Boundary conditions and contact conditions

Constraints on the drop hammer and support are defined in *MAT_RIGID. To ensure that the drop hammer moves exclusively along the Y axis, we constrained the translational freedom of the X and Z axes, as well as the rotational freedom of all axes. Restrict the rotational freedom of the support on Y axis and Z axis and the translational freedom of all axes, and only allow the support to rotate along X axis. To avoid the steel pipe from bouncing at both ends upon impact, we placed two Omega components over each pipe end, as illustrated in Figure 2.

The *CONTACT_AUTOMATIC_SURFACE_TO_SURFACE algorithm was utilized to simulate the contact interactions among various components, comprising the hammer and the outer pipe, the outer pipe and its supporting structure, the innermost pipe and the outer pipe, the centralizer and the outer pipe, and the centralizer and the innermost pipe. The dynamic and static friction coefficients between the outer pipe and the support are set to 0.4. The centralizer was processed into two half-rings and installed onto the exterior of the innermost pipe. A friction coefficient of 1 was set between the innermost pipe and the centralizer, while a friction coefficient of 0 was assigned to all other contact surfaces.

2.3 Finite element validation

Figure 3 illustrates a comparison between the numerical and experimental results of the impact force-time history curve and displacement-time history curve, with reference to findings by Zheng et al. [12]. Additionally, the numerical results from Zheng et al. [12] are presented. The numerical results of the impact force-time history curve match well with the other two curves in Figure 3(a); however, in the displacement-time history curve of Figure 3(b), the numerical results grow faster than the experimental results. This is because the boundary conditions of the numerical simulation are ideal, which is more favorable for the deformation of the pipeline, and this is also the reason why the numerical results of the impact force-time history curve are lower than the experimental results. It can be seen that the finite element simulation results generally agree well with the experimental results, verifying the accuracy of the above modeling method. Consequently, the transverse impact

performance of pipe-in-pipe structures can be analyzed using the finite element model presented in this study.

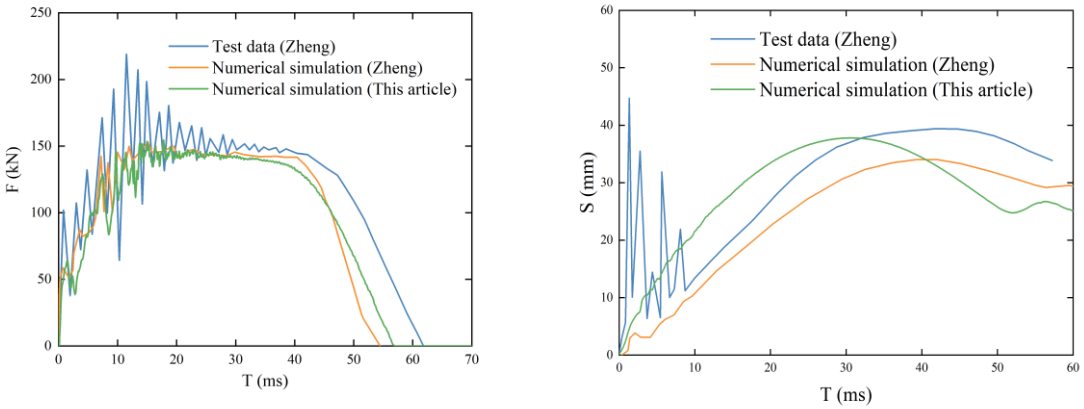

(a) Time history curve of impact force (b) Time history curve of displacement at the mid-span bottom

Figure 3: Impact force-displacement time history curve

3. Full process analysis of impact force on pipe-in-pipe structure

Using the aforementioned modeling approach, a standard finite element analysis model was established for lateral impact on pipe-in-pipe structures. The model was based on the following component parameters: specimen length of 1500mm, outermost pipe external dimension of 141.3mm, outermost pipe wall thickness of 6.55mm, innermost pipe external dimension of 88.9mm, innermost pipe wall thickness of 5.49mm, hammer mass of 1350kg, and impact height of 0.5m.

3.1 Development process of impact force and deformation

To present a comprehensive dynamic response process of the pipe-in-pipe structure under impact, we present in Figures 4 and 5 the time-history curves of impact force, velocity, and displacement of the pipe-in-pipe structure during the impact process.

In order to offer a complete comprehension of the impact process of pipe-in-pipe structures, it is possible to classify it into five distinct stages, which are outlined below.

Stage 1 (OA stage): O is the initial impact moment and A is the moment when the inner and outer pipes first come into contact. When the hammer strikes the outer pipe, according to Figure 4 and Figure 5(a), the impact force rapidly rises to the first peak, the velocity of the top of the outer pipe span increases rapidly, and the velocity of the hammer decreases. At the point where the velocities of the outer pipe span and the hammer are identical, the impact force achieves its utmost magnitude. Subsequently, the hammer and the upper portion of the outer pipe span intersect and descend in unison until the instant that the inner and outer pipes converge. In this stage, the deflection of the outer pipe span of the pipe-in-pipe structure develops, and a noticeable local indentation appears at the impact point.

Stage 2 (AB stage): B is the moment when the displacement of the bottom of the outer pipe span and the local indentation separate obviously. Starting from point A, the inner pipe begins to participate in the entire impact process. As a consequence of the interrelation of the internal and external pipes, the contact stiffness between the hammer and the pipes is elevated, culminating in a more pronounced surge in the striking power. As shown in Figure 5(b), in this stage, the displacement of the bottom of the outer pipe span is similar to the local indentation, and the deformation is still mainly local

deformation.

Oscillation stage (BC stage): C is the point where the acceleration of the hammer is basically consistent with the acceleration of the pipe. Under the impact of the hammer, the velocity of the top of the pipe-in-pipe structure increases, while the velocity of the hammer is relatively small. The contact area between them decreases, and the contact relationship weakens, leading to a decrease in impact force. Due to the effect of the elastic recovery force of the steel pipe, the velocity of the top of the pipe-in-pipe structure gradually decreases, while the velocity of the hammer is relatively large. The contact area between them increases, and the contact relationship becomes stronger, leading to an increase in impact force. This cycle continues until the velocities of the two are basically the same (point C).

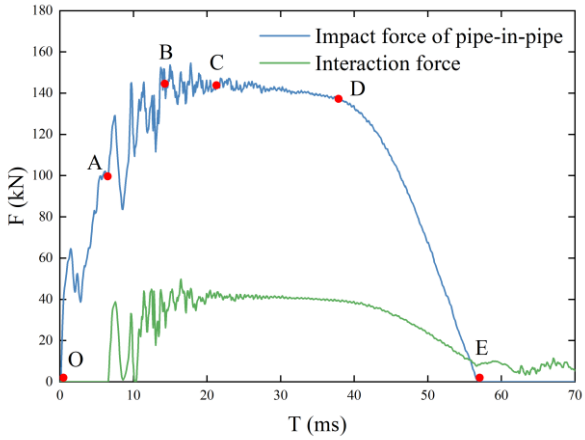

Figure 4: Structural stress-time history curve

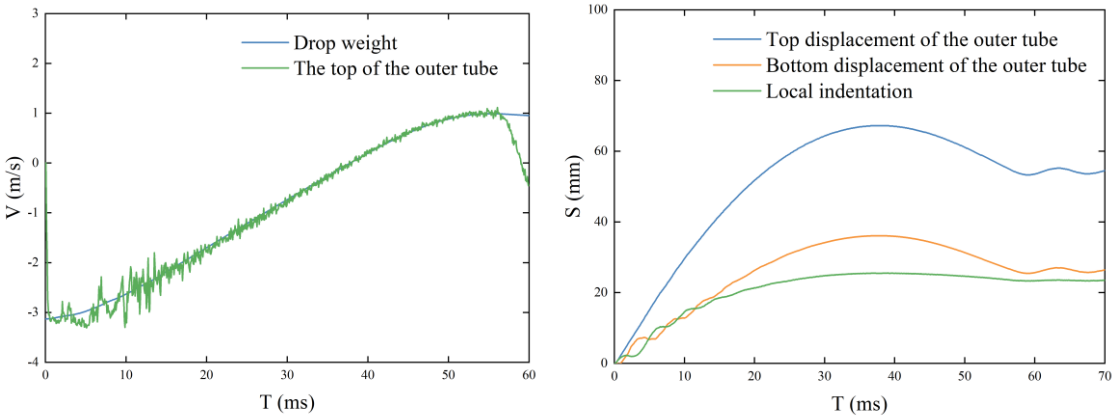

(a) Velocity time history curve (b) Displacement time history curve

Figure 5: Velocity-displacement time history curve

Platform stage (CD stage): at point D, the overall displacement attains its peak value, and the velocity of both the dropping hammer and the outer tube comes to a complete halt. At this stage, the impact force did not fluctuate obviously, and the value remained almost unchanged. The drop hammer and the pipe-in-pipe structure move downwards at uniform speed across the top, and the local dent increases slowly at this stage. When the speed of the drop hammer and the pipe-in-pipe structure drops to zero, the overall deformation reaches the maximum, and this stage ends.

Unloading stage (DE stage): E is the moment when the hammer separates from the outer pipe. As a result of the elastic recovery force, the upper section of the pipe-in-pipe structure bounces upward, propelling the hammer to move upwards in unison. The overall deformation and local indentation of

the steel pipe decrease slightly. As the hammer gradually moves away from the steel pipe, the impact force gradually reduces to zero, indicating the conclusion of this stage.

The interplay force amidst the inner and outer pipes does not drop to zero, but oscillates within a certain range after the impact force-time curve of the hammer and the pipe-in-pipe structure drops to zero, as shown in Figure 4. This is because the inner and outer pipes are impacted at the span, resulting in a small distance between them. After the hammer and the pipe separate, the inner and outer pipes vibrate freely within the elastic range due to collision.

3.2 Energy conversion

As depicted in Figure 6, while undergoing the impact process, a portion of the hammer's kinetic energy is transformed into the kinetic energy of the pipe-in-pipe structure. Another portion of the energy is converted into the strain energy of the same structure. The strain energy of the pipe-in-pipe structure is further divided into elastic strain energy and plastic strain energy. At the start of the release phase, the kinetic energy of both the hammer and the pipe decreases to zero. Furthermore, the total strain energy of the pipe-in-pipe structure reaches its maximum value, exceeding the original kinetic energy of the hammer, with consideration for the gravitational potential energy of the hammer. Then, the strain energy of the inner and outer pipes begins to decrease. Among them, part of the elastic strain energy is converted into the kinetic energy of the hammer, and the other part is converted into the kinetic energy of the pipe-in-pipe structure. As shown in the figure, the pipe-in-pipe structure continuously consumes impact energy through plastic deformation during the impact process. Among them, the plastic strain energy of the outer pipe accounts for 79.1% of the total energy of the component, and the plastic strain energy of the inner pipe accounts for 20.9%. Accordingly, the dissipation of energy in the pipe-in-pipe arrangement during an impact load is due to the plastic deformation of both its inner and outer tubes, with the latter serving as the primary energy dissipation mode.

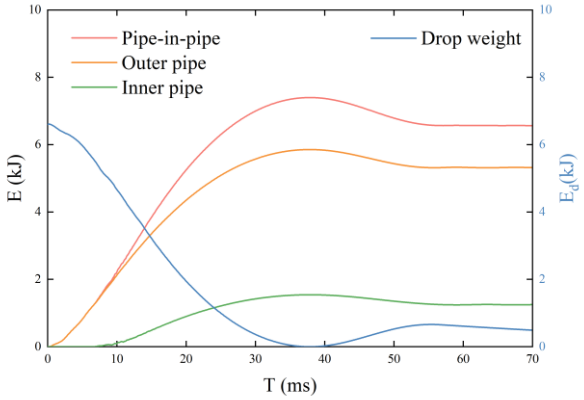

Figure 6: Time history curve of hammer kinetic energy and pipeline strain energy

4. Parameter analysis

The finite element method described above is used to conduct numerical analysis on the main parameters of the pipe-in-pipe structure under lateral impact. The principal factors incorporate the span of the pipe, ratio of diameter for the inner and outer steel pipes, and the ratio of thickness for the inner and outer steel pipes. The mechanical performance is mainly measured by the impact force time-history curve, mid-span overall deformation, local indentation, and energy absorption. The detailed parameters of the component are shown in Table 2.

Table 2: Structural parameters of pipe-in-pipe under different working conditions

Type	Specimen	D_o/mm	t_o/mm	D_i/mm	t_i/mm	L/m	m_d/kg	V/(m/s)	D_i/D_o	t_i/t_o
Span	PIP-1	141.3	6.55	88.9	5.49	1	1350	3.13	0.63	0.84
	PIP-2	141.3	6.55	88.9	5.49	2	1350	3.13	0.63	0.84
	PIP-3	141.3	6.55	88.9	5.49	4	1350	3.13	0.63	0.84
Diameter ratio	PIP-4	141.3	6.55	88.9	5.49	1.5	1350	3.13	0.63	0.84
	PIP-5	141.3	6.55	110	4.33	1.5	1350	3.13	0.78	0.66
	PIP-6	141.3	6.55	120	3.95	1.5	1350	3.13	0.85	0.60
Thickness ratio	PIP-4	141.3	6.55	88.9	5.49	1.5	1350	3.13	0.63	0.84
	PIP-7	141.3	4.79	88.9	8.55	1.5	1350	3.13	0.63	1.78
	PIP-8	141.3	8.36	88.9	2.65	1.5	1350	3.13	0.63	0.32

4.1 Pipeline span.

To examine the impact of pipe span on the pipe-in-pipe structure's lateral impact performance, we chose three sets of the structure with varying spans (1m, 2m, and 4m) for simulation analysis. All other parameters remained constant across the experiments.

The impact force time-history curve is displayed in Figure 7, illustrating the impact of pipe span on the curve. It can be seen that as the pipe span of the pipe-in-pipe structure increases, the plateau force of the component's impact force time-history curve decreases correspondingly, but the impact duration increases. This is because as the span increases, the overall stiffness decreases, leading to a decrease in the plateau force and an increase in the impact duration. The black curve does not have an obvious first peak impact force, which is caused by the contact between the inner and outer pipes before the hammer and the outer pipe reach the same velocity. The impact force time-history curve of the blue curve is 0 for a period of time after reaching the first peak impact force, which is due to the longer pipe span, the lower overall stiffness, and the greater deformation after being impacted, leading to hammer-pipe separation.

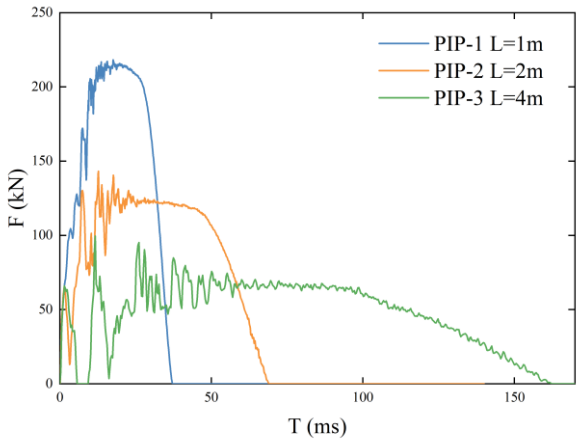

Figure 7: Influence of span on the distribution of impact force

The impact test results displayed in Figure 8 demonstrate the effect of pipe span on the pipe-in-pipe structure's overall deformation and localized depression during lateral impact. It is evident that an increase in span leads to a substantial rise in overall deformation, while localized depression decreases. This is because the increase in pipe length leads to a decrease in overall stiffness, which in turn leads to an increase in overall deformation. The longer the pipe span, the weaker the local effect of the hammer on the pipe, which reduces the local indentation. Therefore, it can be concluded that

increasing the pipe span has a significant impact on the overall deformation, but a minor impact on the local indentation.

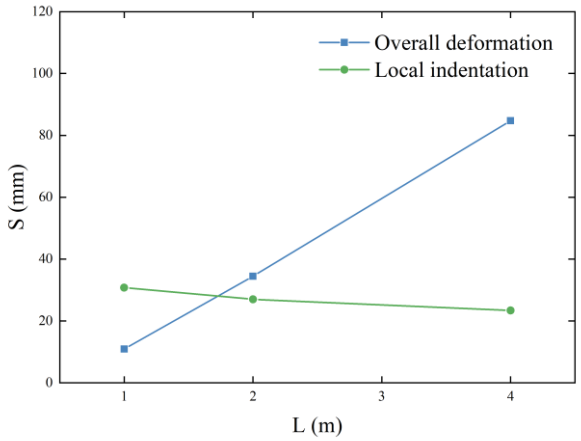

Figure 8: Influence of span on overall deformation and local denting

Wang et al. [24] proposed a dimensionless parameter (EAC) to evaluate the energy absorption capacity of components under impact loads.

$$\mathrm{EAC} = \frac{E_a}{Gw_t} \tag{2}$$

In this context, Ea denotes the energy absorbed by the pipe sample upon impact, whereas G represents the sample's total weight, computed from the steel density and geometric dimensions. Additionally, wt refers to the total bending experienced by the pipe at the point of impact. According to previous research [24], the following energy dissipation mechanisms can be disregarded during impact: (1) hammer rebound; (2) free vibration of the pipe specimen; (3) frictional energy loss between the pipe and its support. As a result, the kinetic energy of the hammer is equivalent to the absorbed impact energy of the pipe-in-pipe structure. Two types of energy dissipation occur within the specimen: energy absorbed by overall bending deformation and energy expended on local indentation.

The pipe-in-pipe structure is composed of an inner pipe and an outer pipe. In the event of sufficient impact energy, the inner and outer pipes collaborate to counteract the external impact. If the impact energy is too small, only the outer pipe will deform, and the inner pipe will not play a role, but the total weight G includes the weight of the inner pipe. In this study, the formula was improved based on Wang et al. [24], and the formula is as follows:

$$\mathrm{EAC} = \frac{E_a}{G_O w_O + G_i w_i} \tag{3}$$

The total weight of the outer pipe and the deflection of the outer pipe at the impact location are denoted as G_O and w_O, respectively. Similarly, the total weight of the inner pipe and the deflection of the inner pipe at the impact location are denoted as G_i and w_i, respectively.

Figure 9 shows the influence of span on the energy absorption of the pipe-in-pipe structure. It can be seen that with the increase of span, the energy absorption of the pipe-in-pipe structure decreases. This is because the impact energy remains constant, and with the increase of span, the weight and deformation of the outer pipe of the pipe-in-pipe structure increase, as well as the weight and deformation of the inner pipe. According to formula (6), the increase of span reduces the energy absorption of the pipe-in-pipe structure. The energy absorption capacity of the pipe-in-pipe structure

with a span of 1 is about 11 times higher than that of the one with a span of 4, which indicates that the span has a significant impact on the energy absorption of the pipe-in-pipe structure.

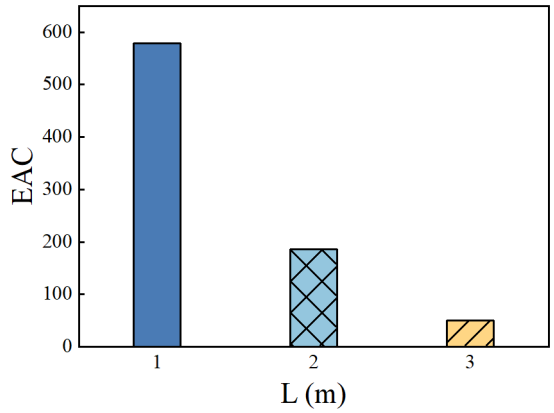

Figure 9: Influence of span on energy absorption

4.2 The effect of the diameter ratio of the inner and outer steel pipes.

In order to investigate the influence of the diameter ratio of the inner and outer steel pipes (D_i/D_o) on the transverse impact performance of the pipe-in-pipe structure, the outer pipe was kept unchanged, and different combinations of inner pipe diameters and wall thicknesses were used to change the ratio of the outer diameter of the inner pipe to the outer diameter of the outer pipe, without changing the steel content of the inner pipe. Three groups of different diameter ratios were selected for simulation, namely 0.63, 0.78, and 0.85.

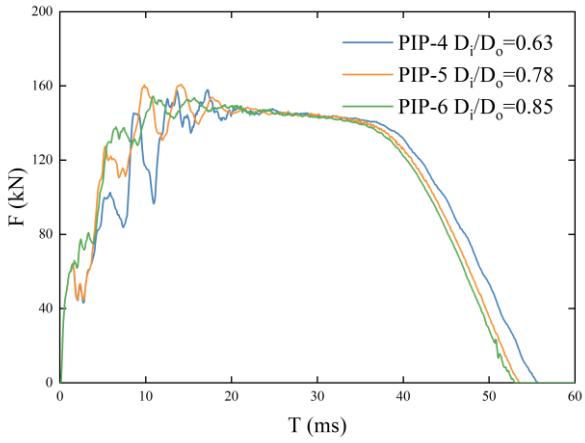

Figure 10: Influence of diameter ratio on the distribution of impact force

The impact force-time curve, depicted in Figure 10, illustrates the impact of the diameter ratio between the inner and outer steel pipes. It is evident from the graph that the plateau force of the impact force-time curve remains relatively steady as the diameter ratio increases. When the outer diameter of the inner pipe increases from 88.9mm to 120mm, which is an increase of 35.0%, the duration of the impact force decreases from 55.65mm to 52.99, which is a decrease of 4.8%. As shown in the figure, before the pipe-in-pipe structure reaches the stable stage, the impact force-time curves of the three components show different oscillation forms. The initial peak impact force is not clearly observed in the green line due to the inner and outer pipes making contact prior to the hammer attaining the same speed as the outer pipe. Then, the yellow line shows a significant increase, which is because the inner and outer pipes participate in the impact together, increasing the structural

stiffness. The yellow and blue lines have the same first peak impact force because they have the same outer pipe, and the inner and outer pipes have not come into contact before the hammer reaches the same speed as the outer pipe. The second peak impact force of the yellow line is significantly higher than that of the blue line because the distance between the inner and outer pipes of the structure corresponding to the yellow line is smaller than that of the blue line, so the inner pipe of the yellow line participates in the impact first, while the inner pipe of the blue line does not come into contact with the outer pipe until the third peak impact force.

In Figure 11, the impact of the diameter ratio between the inner and outer steel pipes on the pipe-in-pipe structure's overall deformation and local indentation is demonstrated. Based on the figure, it is observable that at a diameter ratio of 0.63, the tube-in-tube structure displays an overall deformation of 24.6mm and a local dent of 27.1mm. If the diameter ratio is increased to 0.78, the overall deformation and local dent decrease to 22.7mm and 26.1mm respectively, indicating a 7.7% and 3.7% reduction compared to the 0.63 diameter ratio. Meanwhile, for a diameter ratio of 0.85, the overall deformation and local dent diminish to 22.1mm and 25.8mm respectively, resulting in a 10.2% and 4.8% reduction in comparison to the 0.63 diameter ratio. Based on the analysis above, it is evident that an increase in the tube diameter ratio results in a marginal reduction in both the overall deformation and local indentation of the tube-in-tube structure. The reason for this is that, with an increase in the diameter ratio D_i/D_o, the inner pipe's cross-sectional modulus also increases, leading to an increase in the bending stiffness of the pipe-in-pipe structure. For example, when D_i/D_o increases from 0.63 to 0.85, the cross-sectional modulus of the inner pipe increases from 28268mm4 to 40452mm4.

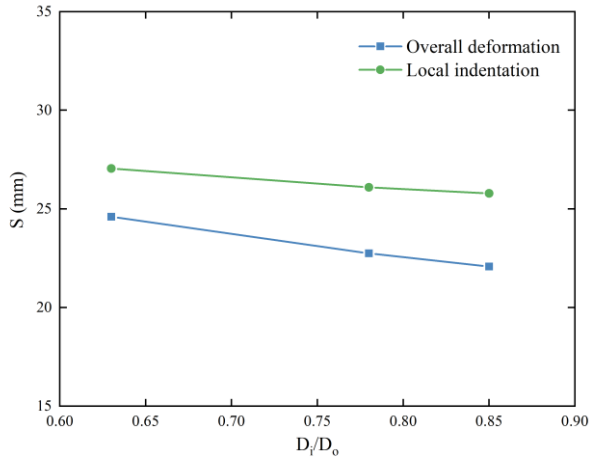

Figure 11: Influence of diameter ratio on overall deformation and local denting

4.3 The effect of the thickness ratio of the inner and outer steel pipes.

To investigate the influence of the thickness ratio of the inner and outer steel pipes on the transverse impact performance of the pipe-in-pipe structure, the outer diameter of the inner pipe and the outer diameter of the outer pipe were kept unchanged during the simulation. The thickness of the inner and outer pipes was changed while keeping the total amount of steel used constant. Three groups of pipe-in-pipe structures with different thicknesses were selected for simulation, and the thickness ratios t_i/t_o were 1.78, 0.84, and 0.32, respectively.

In Figure 12, the impact of the thickness ratio between the inner and outer steel pipes on the transverse impact performance of the pipe-in-pipe structure is demonstrated. As can be seen from the figure, as the thickness ratio decreases, the first peak impact force, the second peak impact force, and the plateau force increase, while the duration of the impact decreases. The reason for this is that, as

the thickness of the outer pipe increases, the local contact stiffness also increases, leading to a rise in the initial peak impact force. During the impact process of the pipe-in-pipe structure, the overall stiffness of the outer pipe dominates. As the thickness of the outer pipe increases, the overall stiffness of the structure also increases, leading to a rise in both the second peak impact force and the plateau force. The increase in impact force results in a shorter duration of the impact force to comply with the law of conservation of momentum.

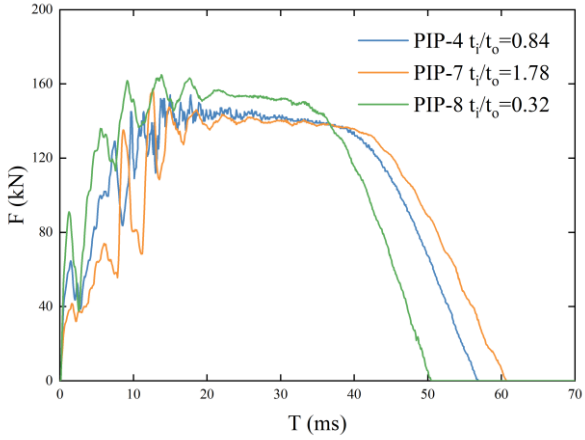

Figure 12: Influence of thickness ratio on the distribution of impact force

In Figure 13, the impact of the thickness ratio between the inner and outer steel pipes on both the overall deformation and local indentation of the pipe-in-pipe structure is presented. Observing the figure, it is clear that at a thickness ratio of 0.32, the overall deformation is 22.6mm and the local dent is 23.1mm. If the thickness ratio increases to 0.84, the overall deformation and local dent increase to 24.6mm and 27.1mm respectively, indicating an 8.8% and 17.3% growth compared to the thickness ratio of 0.32. Similarly, for a thickness ratio of 1.78, the overall deformation and local dent surge to 26.5mm and 31.0mm respectively, resulting in a 17.3% and 34.1% increase in comparison to the thickness ratio of 0.32. Based on the analysis above, it is evident that a decrease in the wall thickness ratio leads to a considerable reduction in both the overall deformation and local dents. This is because the thicker the outer pipe, the greater the overall stiffness, resulting in lower overall deformation; and the thicker the outer pipe, the greater the local stiffness, resulting in lower local indentation.

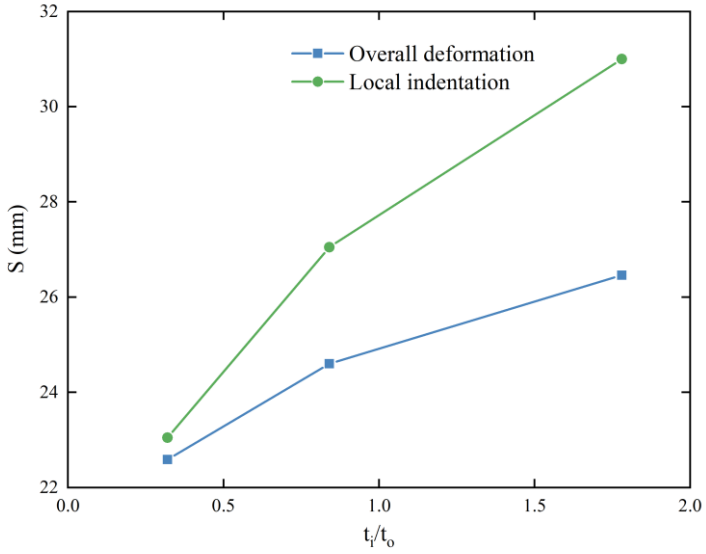

Figure 13: Influence of thickness ratio on overall deformation and local denting

5. Conclusion

The pipe-in-pipe structure was subjected to a comprehensive and parameter analysis under transverse impact, utilizing numerical simulation techniques in this study. The span, diameter, and thickness of the pipeline were analyzed. The main conclusions of this study are as follows:

LS-DYNA is used to establish the finite element model of pipe-in-pipe structure under transverse impact, and the numerical results are verified by the existing experimental data, which proves that the model in this paper can be used to analyze the transverse impact performance of pipe-in-pipe structure.

The process of impact on the pipe-in-pipe structure can be categorized into five stages, namely: the initial stage, the secondary stage, the oscillation stage, the stable stage, and the unloading stage. The initial stage of the impact process is represented by the first stage. During the second stage, there is contact between the inner and outer pipes, which increases their mutual interaction and subsequently enhances the overall and local stiffness of the pipe-in-pipe structure. As a result, the impact force experiences a rapid surge, reaching a new peak in a short timeframe. During the oscillation stage, there is a continuous variation in the contact area between the hammer and the pipe-in-pipe structure, resulting in oscillations that are evident in the impact force-time curve. During the stable stage, both the hammer and the pipe-in-pipe structure, located at the midpoint of the span, move downwards at an equal acceleration rate. Once the velocity drops to zero, the unloading stage commences. At the midpoint of the span, the hammer rebounds and separates from the top of the pipe-in-pipe structure, resulting in the impact force dropping down to zero. The entire impact process comes to a conclusion, allowing the inner and outer pipes to vibrate and collide freely due to the elastic recovery force.

The plastic deformation of both the inner and outer tubes constitutes the energy dissipation mechanism of the tube-in-tube structure when subjected to an impact load. It is noteworthy that the plastic deformation of the outer tube accounts for approximately 80% of the energy dissipation, while the plastic deformation of the inner tube accounts for approximately 20%.

The parameter analysis shows that the span significantly affects the impact resistance of the pipe-in-pipe structure. As the span increases, the overall deformation of the pipeline significantly increases, and energy absorption decreases significantly. The section modulus of the inner tube increases with a larger diameter ratio of the inner and outer tubes. However, the impact resistance of the tube-in-tube structure does not exhibit any significant change with respect to the diameter ratio. If the total steel usage remains constant, enhancing the impact resistance of the pipe-in-pipe structure can be effectively achieved by increasing the thickness ratio between the inner and outer pipes.

References

[1] Vieth PH, Roytman I, Mesloh RE, et al. Analysis of DOT reportable incidents for gas transmission and gathering pipelines--January 1, 1985 through December 31, 1994. Final report [J]. 1996.

[2] Jones N, Birch SE, Birch RS, et al. An experimental study on the lateral impact of fully clamped mild steel pipes [J]. Proceedings of the Institution of Mechanical Engineers, Part E: Journal of Process Mechanical Engineering, 1992; 206: 111-127.

[3] Jones N, Shen WQ. A theoretical study of the lateral impact of fully clamped pipelines [J]. Proceedings of the Institution of Mechanical Engineers, Part E: Journal of Process Mechanical Engineering, 1992; 206:129-146.

[4] Chen K, Shen WQ. Further experimental study on the failure of fully clamped steel pipes [J]. International journal of impact engineering, 1998; 21:177-202.

[5] Shen WQ, Chen KS. An investigation on the impact performance of pipelines [J]. International journal of crashworthiness, 1998; 3:191-210.

[6] Cerik BC, Shin HK, Cho SR. A comparative study on damage assessment of tubular members subjected to mass impact [J]. Marine Structures, 2016; 46: 1-29.

[7] Zhu L, Liu Q, Jones N, et al. Experimental study on the deformation of fully clamped pipes under lateral impact [J].

International Journal of Impact Engineering, 2018; 111: 94-105.
[8] Zhang R, Zhi X, Fan F. Plastic behavior of circular steel tubes subjected to low-velocity transverse impact [J]. International Journal of Impact Engineering, 2018; 114:1-19.
[9] Liu K, Liu B, Wang Z, et al. An experimental and numerical study on the behaviour of tubular components and T-joints subjected to transverse impact loading [J]. International journal of impact engineering, 2018; 120: 16-30.
[10] Lu Y, Liu K, Wang Z, et al. Dynamic behavior of scaled tubular K-joints subjected to impact loads [J]. Marine Structures, 2020; 69: 102685.
[11] Kyriakides S, Vogler T J. Buckle propagation in pipe-in-pipe systems: Part II. Analysis [J]. International journal of solids and structures, 2002; 39: 367-392.
[12] Kyriakides S. Buckle propagation in pipe-in-pipe systems: Part I. Experiments [J]. International journal of solids and structures, 2002; 39: 351-366.
[13] Gong S, Li G. Buckle propagation of pipe-in-pipe systems under external pressure [J]. Engineering Structures, 2015; 84: 207-222.
[14] Bi K, Hao H. Using pipe-in-pipe systems for subsea pipeline vibration control [J]. Engineering Structures, 2016; 109: 75-84.
[15] Nikoo HM, Bi K, Hao H. Effectiveness of using pipe-in-pipe (PIP) concept to reduce vortex-induced vibrations (VIV): Three-dimensional two-way FSI analysis[J]. Ocean Engineering, 2018; 148: 263-276.
[16] Zheng J, Palmer A, Lipski W, et al. Impact damage on pipe-in-pipe systems[C]//The Twenty-second International Offshore and Polar Engineering Conference. OnePetro, 2012.
[17] Zheng JX, Palmer A, Brunning P. Overtrawlability and mechanical damage of pipe-in-pipe [J]. Journal of Applied Mechanics, 2014; 81: 31006.
[18] Zheng J, Palmer A, Brunning P, et al. Method to assess the overtrawlability of Pipe-in-Pipe[C]//Offshore Technology Conference-Asia. OnePetro, 2014.
[19] Zheng J, Palmer A, Brunning P, et al. Indentation and external pressure on subsea single wall pipe and pipe-in-pipe [J]. Ocean engineering, 2014; 83: 125-132.
[20] Gao X, Shao Y, Xie L, et al. Behavior of API 5L X56 submarine pipes under transverse impact[J]. Ocean Engineering, 2020; 206:107337.
[21] Gao X, Shao Y, Chen C, et al. Experimental and numerical investigation on transverse impact resistance behaviour of pipe-in-pipe submarine pipelines after service time [J]. Ocean Engineering, 2022; 248: 110868.
[22] Jones N. Structural impact [M]. Cambridge university press, 2011.
[23] Abramowicz W, Jones N. Dynamic axial crushing of square tubes [J]. International Journal of Impact Engineering, 1984; 2:179-208.
[24] Wang Y, Qian X, Liew JYR, et al. Experimental behavior of cement filled pipe-in-pipe composite structures under transverse impact [J]. International Journal of Impact Engineering, 2014; 72: 1-16.